Fast Non-minimal Solvers for Planar Motion Compatible Homographies

Marcus Valtonen Örnhag
Centre for Mathematical Sciences, Lund University, Lund, Sweden

Keywords: Planar Motion, Homography, Polynomial Solver, Trajectory Recovery, Visual Odometry.

Abstract: This paper presents a novel polynomial constraint for homographies compatible with the general planar motion model. In this setting, compatible homographies have five degrees of freedom—instead of the general case of eight degrees of freedom—and, as a consequence, a minimal solver requires 2.5 point correspondences. The existing minimal solver, however, is computationally expensive, and we propose using non-minimal solvers, which significantly reduces the execution time of obtaining a compatible homography, with accuracy and robustness comparable to that of the minimal solver. The proposed solvers are compared with the minimal solver and the traditional 4-point solver on synthetic and real data, and demonstrate good performance, in terms of speed and accuracy. By decomposing the homographies obtained from the different methods, it is shown that the proposed solvers have future potential to be incorporated in a complete Simultaneous Localization and Mapping (SLAM) framework.

1 INTRODUCTION

Polynomial systems of equations naturally arise in the field of computer vision, as an instrument of encoding geometric properties and other constraints one wishes to impose on the desired output. To solve a general system of polynomial equations, is, however, a task requiring certain endeavour, in order to produce a solver that is sufficiently fast and numerically stable.

In this paper we will investigate methods for Visual Odometry (VO), where the expected input is a sequence of images from a camera mounted on a mobile platform. The goal is to estimate the egomotion of the platform, in indoor environments or other challenging scenes containing planar surfaces. This is done by considering homography based methods, where we enforce the general planar motion model. By imposing these constraints, thus lowering the total degrees of freedom of the motion parameters, it is possible to navigate robustly in scenes containing planar structures, which are problematic for VO systems where a general structure of the scene is assumed. It does, however, introduce a number of non-trivial polynomial constraints, and a proper framework for dealing with them must be employed.

The major contributions are:

i. To derive a new polynomial constraint for the general planar motion model, and show that this, together with known constraints, are sufficient conditions for compatibility.

ii. To develop a series of non-minimal solvers to enforce a weaker form of the general planar motion model, with a similar accuracy as the existing minimal solver, at a greatly reduced speed.

iii. To demonstrate that pre-optimization on an early stage in the intended VO pipeline, by enforcing the general planar motion model on the homographies (but not a sequence of homographies), do not necessarily give an increased performance.

2 RELATED WORK

Planar motion models with different complexity have been considered to increase robustness of navigation systems, by decreasing the total number of parameters to be recovered. In (Ortín and Montiel, 2001) a mobile platform with a single camera was considered, where the optical axis was parallel to the floor. This made it possible to parameterize the essential matrix by imposing a planar motion model with two translational components and a single rotational component. They propose a linear 3-point algorithm and a non-linear 2-point algorithm; however, only the direction of the translation can be recovered using their method. Furthermore, the alignment of the optical axis with the floor is not feasible for real-life applications. The same geometrical setup was considered in (Chen and Liu, 2006), but the algorithm was extended to stereo vision.

Örnhag, M.
Fast Non-minimal Solvers for Planar Motion Compatible Homographies.
DOI: 10.5220/0007258600400051
In *Proceedings of the 8th International Conference on Pattern Recognition Applications and Methods (ICPRAM 2019)*, pages 40-51
ISBN: 978-989-758-351-3

The fundamental matrix (or the essential matrix in the calibrated case) have been successfully used in many computer vision and robotics applications. Despite many promising navigation systems for general scenes, such methods will not work well under planar motion, as it is known to be ill-conditioned (Hartley and Zisserman, 2004; Torr et al., 1998). As planar structures are common in man-made environments, researchers have considered alternative methods, many of which are based on inter-image homographies.

In (Hajjdiab and Laganière, 2004) a planar motion model with one tilt parameter was considered, and they proposed a method for estimating all motion parameters. By allowing an arbitrary tilt about the floor normal Liang and Pears showed that the eigenvalues of the homography matrix is related to the rotation of the mobile platform, regardless of the tilt (Liang and Pears, 2002). Their method, however, did not estimate the tilt parameters.

The method proposed in (Wadenbäck and Heyden, 2013; Wadenbäck and Heyden, 2014) estimates the full set of motion parameters for the general planar motion model with five degrees of freedom by decoupling the overhead tilt using an iterative scheme. From the same model assumption, but employing a dense matching scheme, Zienkiewicz and Davison devise a non-linear optimization scheme for the full set of motion parameters (Zienkiewicz and Davison, 2015).

Without enforcing any model constraints, a general homography has eight degrees of freedom; however, a homography compatible with the general planar motion model only has five, as it is determined (up to scale) by the motion parameters. Due to the automated process of extracting and matching keypoints, homography solvers often employ RANSAC, or similar frameworks, to reject outliers. The number of iterations N required to select a set of keypoints only containing inliers is dependent on the size of the subset of keypoints n, the desired probability p and inlier ratio w, by the well-known relation $N = \log(1-p)/\log(1-w^n)$ (Fischler and Bolles, 1981). One way of increasing the speed of such an algorithm is to reduce the necessary number of iterations, i.e. to create a solver that only uses the minimal number of point correspondences needed for the application. Such a solver is known as a *minimal solver*. In line with this argument, it is natural to consider a minimal homography solver compatible with the planar motion model, which has been constructed in (Wadenbäck et al., 2016). They parameterize the homography as a linear combination of the basis elements of the null space of the corresponding DLT system, with 2.5 DLT constraints, and construct eleven quartic constraints on the homography matrix, which results in a system of eleven quartic equations in three variables. By generating the corresponding ideal, a basis for the quotient space can be constructed and the original problem solved by employing the action matrix method (Möller and Stetter, 1995). Their derivation involves steps of manual selection of basis monomials, which is a time-consuming task.

In (Kukelova et al., 2008) an automatic generator for polynomial systems was introduced, and several improvements have been made in recent years to increase the performance, see e.g. (Larsson and Åström, 2016; Larsson et al., 2017a; Larsson et al., 2017b; Larsson et al., 2018b). Such methods have been successfully used in several computer vision applications, e.g. (Ventura et al., 2014; Zheng et al., 2013).

Minimal solvers permit intrinsic constraints to be enforced on the solutions, while minimizing the number of necessary iterations in a RANSAC framework; however, there are cases when the minimal solvers are sensitive to noise, see e.g. (Triggs, 1991), or when the complexity of minimal solver is large, thus making it very slow, see e.g. (Larsson et al., 2018a). Under such circumstances constructing a non-minimal solver is a viable option.

3 PLANAR MOTION

3.1 Problem Geometry

In this paper we consider a mobile platform with a single camera directed towards the floor. The world coordinate system is chosen such that the camera moves in the plane $z = 0$. The scale is fixed by assuming the ground plane is positioned at $z = 1$, which is illustrated in Figure. 1.

We employ the parameterization used in (Wadenbäck and Heyden, 2013), where the camera matrices for two consecutive poses A and B, are given by

$$\begin{aligned} \boldsymbol{P}_A &= \boldsymbol{R}_{\psi\theta}[\boldsymbol{I} \mid \boldsymbol{0}], \\ \boldsymbol{P}_B &= \boldsymbol{R}_{\psi\theta}\boldsymbol{R}_{\phi}[\boldsymbol{I} \mid -\boldsymbol{t}], \end{aligned} \tag{1}$$

where $\boldsymbol{R}_{\psi\theta}$ is a rotation θ about the y-axis followed by a rotation ψ about the x-axis. As the mobile platform rotates about the plane normal (or z-axis) the angle ϕ varies, corresponding to $\boldsymbol{R}_{\phi}$. The translation of the mobile platform is modelled by a translation vector $\boldsymbol{t} = (t_x, t_y, 0)^T$. It follows that the inter-image homography is given by

$$\boldsymbol{H} \sim \boldsymbol{R}_{\psi\theta}\boldsymbol{R}_{\phi}\boldsymbol{T}_{\boldsymbol{t}}\boldsymbol{R}_{\psi\theta}^T, \tag{2}$$

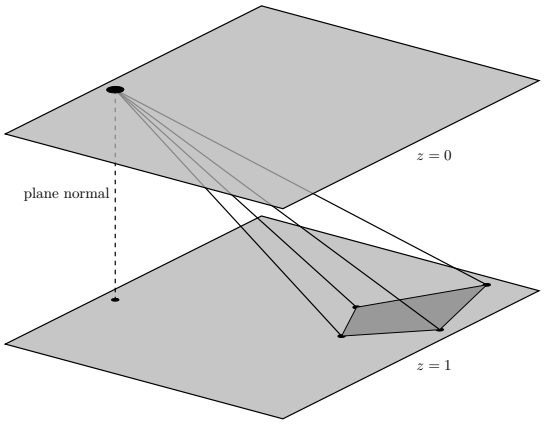

Figure 1: The problem geometry considered in this paper. The camera moves in the plane $z = 0$, and is tilted about the y-axis an unknown angle θ, followed by a rotation about the x-axis by an unknown angle ψ, The ground floor is positioned at $z = 1$.

where $\boldsymbol{T_t} = \boldsymbol{I} - \boldsymbol{t}\boldsymbol{n}^T$ is the translation matrix corresponding to the translation $\boldsymbol{t}$, and $\boldsymbol{n} = (0, 0, 1)^T$ is a floor normal. The homography matrix can be made unique by imposing $\det \boldsymbol{H} = 1$, which will be assumed throughout the paper.

3.2 Parameter Recovery

In (Wadenbäck and Heyden, 2013) an algorithm for recovering the full set of motion parameters for the general planar motion model was suggested. Their approach is to separate the overhead tilt $\boldsymbol{R}_{\psi\theta}$ from the nonconstant motion parameters. This can be achieved using a coordinate-descent like optimization scheme, where one of the tilt angles are fixed and the other is solved for. A more robust version by the same authors was introduced in (Wadenbäck and Heyden, 2014) by using more than one homography, and incorporating the assumption of a fixed overhead tilt throughout the entire trajectory of the mobile platform.

4 COMPATIBLE HOMOGRAPHIES

The *Direct Linear Transform* (DLT) equations for a pair of point correspondences $\boldsymbol{x} \leftrightarrow \hat{\boldsymbol{x}}$, where $\boldsymbol{x} = (x, y, 1)^T$ and $\hat{\boldsymbol{x}} = (\hat{x}, \hat{y}, 1)^T$ is given by

$$\begin{bmatrix} \boldsymbol{0} & -\boldsymbol{x}^T & \hat{y}\boldsymbol{x}^T \\ \boldsymbol{x}^T & \boldsymbol{0} & -\hat{x}\boldsymbol{x}^T \\ -\hat{y}\boldsymbol{x}^T & \hat{x}\boldsymbol{x}^T & \boldsymbol{0} \end{bmatrix} \begin{bmatrix} \boldsymbol{h}_1 \\ \boldsymbol{h}_2 \\ \boldsymbol{h}_3 \end{bmatrix} = \boldsymbol{0}, \tag{3}$$

where $\boldsymbol{h}_k^T$ is the k:th row of the homography matrix $\boldsymbol{H}$. It is only necessary to consider the first two rows of the DLT system matrix in (3), as the third is a linear combination of the others. We will use these equations to parameterize the null space of the homography matrix $\boldsymbol{H}$ in Section 6.

We will introduce some notation from algebraic geometry in order to outline the method employed to create the polynomial solvers we will consider in this paper.

4.1 The Action Matrix Method

Consider a polynomial system of equations

$$\begin{aligned} f_1(\boldsymbol{x}) &= 0, \\ &\vdots \\ f_s(\boldsymbol{x}) &= 0\,. \end{aligned} \tag{4}$$

The set of all solutions to (4), is known as an affine variety, and denoted $\boldsymbol{V}(f_1, \ldots, f_s) \subset \mathbb{C}[\boldsymbol{x}]$, where $\mathbb{C}[\boldsymbol{x}]$ is the set of polynomials in $\boldsymbol{x}$ with coefficients in $\mathbb{C}$. The ideal generated by $f_1, \ldots, f_s$, is denoted

$$\langle f_1, \ldots, f_s \rangle = \left\{ \sum_{i=1}^{s} h_i f_i \,:\, h_1, \ldots, h_s \in \mathbb{C}[\boldsymbol{x}] \right\}. \tag{5}$$

Every ideal of $\mathbb{C}[\boldsymbol{x}]$ is finitely generated, thus, the polynomial system of equations (4) is defined by the generated ideal.

Under the assumption that the system has finitely many solutions, $I = \langle f_1, \ldots, f_s \rangle$ is zero-dimensional and the quotient space $A = \mathbb{C}[\boldsymbol{x}]/I$ is finite dimensional (Cox et al., 2005). Let $[f] = \{f + h \mid h \in I\}$ denote the coset and consider the operator $T_f : A \longrightarrow A$, defined by $T_f([g]) = [fg]$. Since the quotient space A is finite-dimensional this operation can be represented by a matrix $\boldsymbol{M}_f$, which is known as the *action matrix*. Furthermore, select a monomial basis for A, which we denote $\mathcal{B} = \{[\boldsymbol{x}^{\alpha_j}]\}_{j \in J}$. Typically, such a basis is obtained by using an improved version of Buchberger's algorithm. When the action matrix $\boldsymbol{M}_f = (m_{ij})$ acts on the basis elements a linear combination of the monomials forming the basis is obtained,

$$T_f([\boldsymbol{x}^{\alpha_j}]) = [f\boldsymbol{x}^{\alpha_j}] = \sum_{i \in J} m_{ij} [\boldsymbol{x}^{\alpha_i}]\,. \tag{6}$$

Consequently, for $\boldsymbol{x} \in V(I)$,

$$f(\boldsymbol{x})\boldsymbol{x}^{\alpha_j} = \sum_{i \in J} m_{ij} \boldsymbol{x}^{\alpha_i}\,. \tag{7}$$

The basis $\mathcal{B}$ may be represented by a vector $\boldsymbol{b}$, and since that (7) must hold for all basis elements, the problem can be reduced to an eigenvalue problem, given by

$$f(\boldsymbol{x})\boldsymbol{b}(\boldsymbol{x}) = \boldsymbol{M}_f^T \boldsymbol{b}(\boldsymbol{x})\,. \tag{8}$$

By multiplying (4) by a set of monomials an equivalent, but larger problem is obtained. The problem of finding a suitable monomial basis remains, and there is no exact criterion for doing so; however, it is desirable to find the minimal set of monomials to make the problem solvable (or numerically stable). The coefficient matrix of the expanded matrix is known as an *elimination template*, and numerous attempts of optimizing these have been made, see e.g. (Kukelova et al., 2008; Larsson and Åström, 2016; Larsson et al., 2017b; Larsson et al., 2018b).

4.2 Necessary Conditions

In (Wadenbäck et al., 2016) eleven quartic constraints for planar motion compatible homographies were derived, and used to create a minimal solver. These constraints were experimentally obtained by randomly generating points on the manifold defining the planar motion compatible homographies. In order to be able to work over a finite field, the rotation matrices were constructed using Pythagorean triplets, hence integer versions of the problem were obtained. By doing so, the coefficients for the polynomials could be found. With this approach, however, one cannot rule out the existence of higher order polynomials, and thus, sufficiency cannot be proven. We will approach this differently in the next Section.

5 SUFFICIENT CONDITIONS

In this section, we will show that the eleven quartic constraints discussed in Section 4.2 are necessary but not sufficient. Furthermore, we show that by adding a sixth degree polynomial to the existing quartic constraints one may guarantee sufficiency. This is done by a novel parameterization, which allows one to efficiently compute the relevant elimination ideal.

Instead of considering the original camera matrices (1), choose the coordinate system such that $\boldsymbol{P}_A = [\boldsymbol{I} \,|\, \boldsymbol{0}]$, giving $\boldsymbol{P}_B = [\boldsymbol{R}_{\boldsymbol{n}}(\phi) \,|\, -\boldsymbol{t}]$. This can be thought of as travelling parallel to an unknown plane, as is illustrated in Figure 2, hence the homography can be parameterized as

$$\boldsymbol{H} = \boldsymbol{R}_{\boldsymbol{n}}(\phi) + \boldsymbol{t}\boldsymbol{n}^T, \tag{9}$$

where $\boldsymbol{t} = (t_x, t_y, t_z)^T$ is a translation vector orthogonal to the plane normal $\boldsymbol{n} = (n_x, n_y, n_z)^T$. The constraint of travelling parallel to the plane can be expressed as $\boldsymbol{t} \cdot \boldsymbol{n} = 0$ and, to fix the scale, one may assume that $\|\boldsymbol{n}\|^2 = 1$.

Let $\boldsymbol{q} = (1, q_x, q_y, q_z)$ be a unit quaternion, then $\boldsymbol{n} = (q_x, q_y, q_z)$ and the corresponding rotation matrix $\boldsymbol{R} = \boldsymbol{R}(\boldsymbol{q})$. Let the ideal generated by $\lambda\boldsymbol{H} - \boldsymbol{R}(\boldsymbol{q}) - \boldsymbol{t}\boldsymbol{n}^T = 0$ and $\boldsymbol{t} \cdot \boldsymbol{n} = 0$ be denoted I, then we seek the elimination ideal $I \cap \mathbb{K}[\boldsymbol{H}]$, for some suitable field $\mathbb{K}$. Over a finite field, this can be done using Macaulay2 (Grayson and Stillman, 2018). This results in the eleven quartic constraints found in (Wadenbäck et al., 2016) and an additional sixth degree polynomial[1]. The constraints were symbolically verified to hold over $\mathbb{C}$ as well.

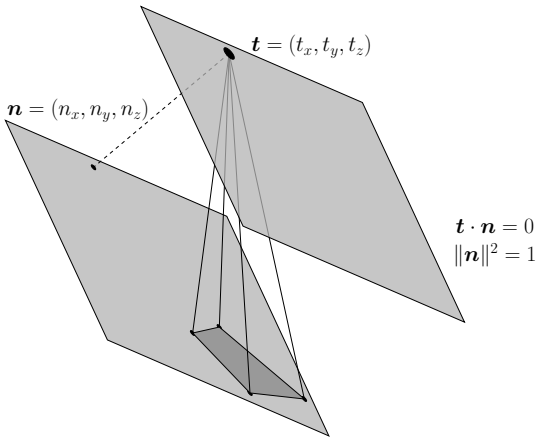

Figure 2: Revised problem geometry. The camera moves parallel to an unknown plane defined by a normal vector $\boldsymbol{n}$ of unit length.

6 NON-MINIMAL SOLVERS

In this section we consider different non-minimal solvers as an alternative to the minimal solver proposed in (Wadenbäck et al., 2016). The main reason we consider such solvers is due to the minimal solver being computationally expensive. Also, there is no advantage between a 2.5-point solver and a 3-point solver, in terms of the number of iterations required to select a subset of inliers with a certain probability—this is a favourable trait, compared to the standard 4-point DLT solver. Furthermore, we would like to explore different methods using the novel sixth degree polynomial, derived in Section 5. Lastly, and most importantly for practical applications, the condition that the overhead tilt remains constant is not enforced by using any of the described method, but is achieved at a later step in the VO pipeline. Therefore, it is uncertain if pre-optimizing the homographies will yield a better end result.

In this paper we construct four different non-minimal solvers

3pt(4+4) a 3-point solver enforcing two quartic

[1] See the Appendix for implementation details.

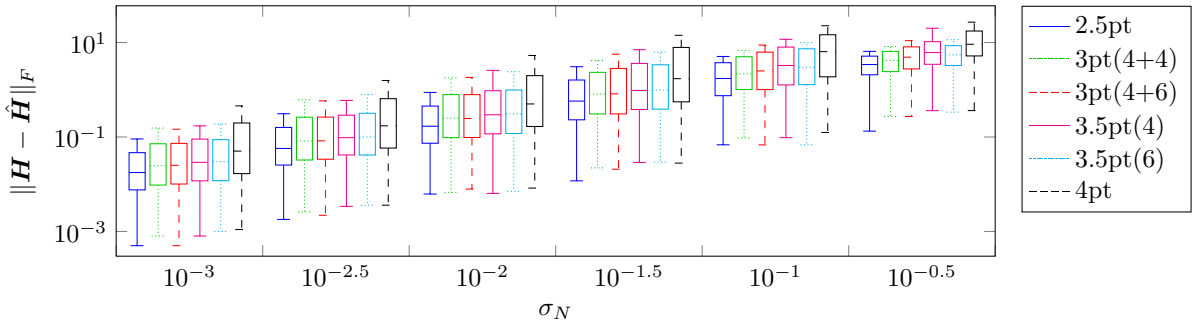

Figure 3: Distribution of homography error in the Frobenius norm for different noise levels σ_N. The proposed non-minimal solvers have a median error between the 2.5-point solver and DLT for all noise levels considered in the experiment.

constraints,

3pt(4+6) a 3-point solver enforcing one quartic constraint and the sextic constraint,

3.5pt(4) a 3.5-point solver enforcing one quartic constraint,

3.5pt(6) a 3.5-point solver enforcing the sextic constraint.

These solvers were chosen because they enforce a weaker version of the general planar motion model in different ways. Furthermore, we will compare with the minimal solver and the standard 4-point DLT solver.

From the eleven quartic constraints the first two w.r.t. DEGLEX was chosen to construct the solvers; however, this was only chosen for reproducibility, as empirical tests showed that the size of the elimination template did not change by considering other pairs. Similarly, when constructing the 3pt(4+6) and 3.5pt(4) solvers only the first quartic constraint was chosen.

6.1 Parameterizing the Null Space

The standard approach, which we will utilize, is to parameterize the null space, and use the parameterization to obtain the desired polynomial system of equations. Using three DLT constraints (3) the homography matrix $\boldsymbol{H}$ has a 3-dimensional null space, hence can be parameterized as

$$\boldsymbol{H}(\boldsymbol{z}) = \boldsymbol{H}_0 + z_1\boldsymbol{H}_1 + z_2\boldsymbol{H}_2\,. \tag{10}$$

Similarly, for the 3.5-point solvers, the null space is two-dimensional, leaving a single variable. For such systems, the action matrix method is replaced with a simpler root finding algorithm, involving the companion matrix (Trefethen and Bau, 1997). In both cases this allow the homography to be written as a function $\boldsymbol{H} = \boldsymbol{H}(\boldsymbol{z})$, and inserted to any of the polynomial constraints f_i, yields an equation $f_i(\boldsymbol{H}(\boldsymbol{z})) = 0$ in the variable $\boldsymbol{z}$. For the 3-point solvers a system of two equations are obtained, and the corresponding ideal $I = \langle f_1, f_2 \rangle$ can be studied. The number of basis elements in the quotient space determines the number of solutions (for non-degenerate configurations).

For the 3pt(4+4) solver the basis consists of 16 elements, hence the polynomial system of equations has at most 16 solution. By using the automatic generator proposed by (Larsson et al., 2017a) an elimination template of size 20×36 was constructed. Due to the increased complexity of the sextic constraint the 3pt(4+6) solver has in general 24 solutions, and the corresponding elimination template is of size 31×55. Furthermore, the coefficients in the elimination template are significantly more complex.

7 EXPERIMENTS

7.1 Noise Sensitivity

In order to be comparable with the study of noise sensitivity for the minimal solver proposed in (Wadenbäck et al., 2016), the same setup was used. Homographies $\boldsymbol{H}_j$ compatible with the general planar motion model were generated together with randomly generated keypoints $\boldsymbol{x}_k$ with zero mean and unit variance. The image correspondences $\hat{\boldsymbol{x}}_k \sim \boldsymbol{H}_j\boldsymbol{x}_k$ were computed and normalized to unit variance. To simulate noise, a normal distributed term was added to $\boldsymbol{x}_k$ and $\hat{\boldsymbol{x}}_k$ with standard deviation σ_N. The homographies obtained from the solvers were normalized such that $\det \boldsymbol{H}_j = 1$, and the error measured in the Frobenius norm of the difference between the ground truth and the estimated homographies, see Figure 3. The median sensitivity to noise of the proposed solvers is between the corresponding values for the 2.5-point solver and the 4-point (DLT) solver for all noise levels, which indicates a trade-off between accuracy and speed.

Secondly, we generate a sequence of homographies compatible with the general planar motion model, and use the method described in Section 3.2 to recover the motion parameters. For this example the noise level was kept constant while increasing the number of homographies used to estimate the motion parameters. For $\sigma_N = 10^{-2}$ the results are shown in Figure 4. The results for the other motion parameters, and different standard deviation σ_N follow the same trend, and can be found in the Appendix. Note, that the mean error for the 3-point solvers are close to the minimal solver after approximately 15 homographies are used.

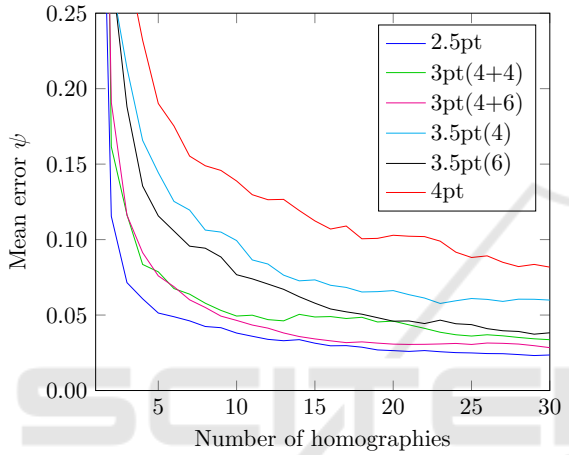

Figure 4: Mean error for ψ (in degrees) for 100 iterations.

7.2 Speed Evaluation

The solvers were implemented in MATLAB, with mex-compiled C++ routines. For a fair comparison, the 2.5-point method and the 4-point (DLT) method were also constructed this way. The 2.5-point method was generated using the automatic solver by Larsson et al. (Larsson et al., 2017a), thus producing a different elimination template than the one proposed in (Wadenbäck et al., 2016).

The execution time of the solvers was tested on a standard laptop computer, and the measurements include the complete process of estimating a homography, i.e. staring from point correspondences, the construction of the DLT system, extracting the null space through SVD, and—except for the 4-point solver—the parameter estimation for the basis elements of the null space, and construction of putative homographies.

In Table 1 the timing comparison is shown, and the speed-up between the minimal 2.5-point solver and 3pt(4+4) solver is clear, however, in terms of speed the traditional 4-point solver is faster. In a complete RANSAC framework, however, the 3-point solver and the 4-point solver is closer in terms of speed, due to the 4-point solver requiring more iterations to achieve the same probability of selecting a subset containing only inliers.

Table 1: Mean execution time for 10,000 randomly generated problems.

Solver	Exec. time (ms)
2.5pt	0.7960
3pt(4+4)	0.1334
3pt(4+6)	1.6161
3.5pt(4)	0.0344
3.5pt(6)	0.2919
4pt	0.0334

When enforcing the sixth degree polynomial in the 3-point solver the number of solutions increase, hence the corresponding elimination template. Furthermore, the complexity of the coefficients increase, and this holds true in the case of the 3.5-point solvers as well, which is why the execution time is faster without the sextic constraint.

7.3 Synthetic Image Evaluation

A sequence of synthetic images were generated, compatible with the general planar motion model, by cropping out images from a high-resolution image. In order to simulate the overhead tilt the original image was transformed prior to cropping it. An elliptic path containing 49 images were generated, as well as the corresponding ground truth.

The homographies were computed by extracting and matching SURF features. In order to estimate the trajectory, the homographies were decomposed using the method described in Section 3.2. The point correspondences were normalized prior to estimating the homographies to increase numerical stability. The extracted motion parameters were compared to the ground truth. Due to the random nature of the RANSAC, the recovered parameters were averaged over 100 iterations. The results are shown in Table 2.

Table 2: Mean estimation error for the motion parameters for the synthetic image test averaged over 100 iterations. Angles are measured in degrees, and translation in pixels. The best performance is in bold.

	2.5pt	**3pt(4+4)**	**3pt(4+6)**	**3.5pt(4)**	**3.5pt(6)**	**4pt**
ψ	0.0035	0.0005	0.0029	**0.0004**	0.0006	0.0007
θ	0.0019	0.0006	0.0013	**0.0005**	0.0006	0.0007
ϕ	1.08	**0.68**	0.77	0.76	0.73	0.86
t	20.36	**6.85**	10.49	6.99	7.65	11.29

We observe that the minimal solver is no longer producing the best results, and one may note the ad-

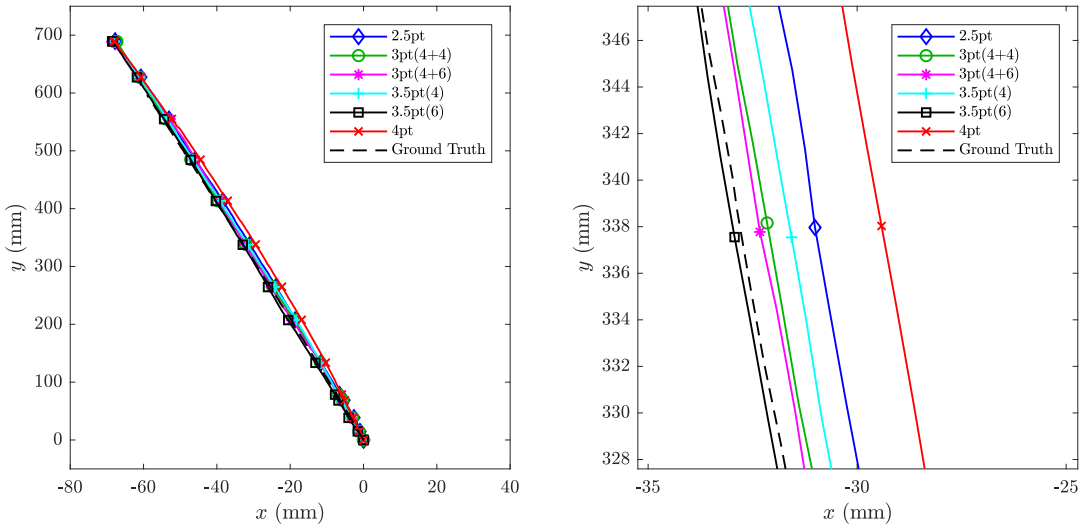

Figure 5: The sequence of the planar motion test set. The entire trajectory is shown to the left, and to the right a zoomed in version showing the difference in estimates by using different solvers. The total sequence contains 320 images.

vantage of using non-minimal solvers. The exact reason why this phenomenon arises when considering synthetically generated sequences of images and not synthetically generated sequences of homographies is hard to pinpoint; however, we note the following differences: (a) the matched points, which are the input to the solvers do not follow a Gaussian distribution, and (b) when analyzing the numerical rank of the elimination template it often has less than full rank, which is not the case for the Gaussian distributed noise. This holds true regardless of whether one normalizes the image points or not. (c) the numerical rank of the other elimination templates do not change when going from synthetic homographies to synthetic images.

7.4 Planar Motion Evaluation

The following experiments were conducted using a mobile robot with omnidirectional wheels, of model Fraunhofer IPA rob@work. A camera was mounted, directed towards the floor, and the ground truth was measured using a Nikon Metrology K600 optical tracking system. The system has an absolute accuracy of 100 μm. In Figure 6 example images from one of the sequences are shown. In the first test sequences the robot travels along a straight line, while keeping the orientation constant.

The same approach for computing the homographies in Section 7.3, after first compensating for geometric distortion. The results are shown in Figure 5, and more test results are shown in the Appendix. Note, that the minimal solver and the 4-point solver are the ones to deviate the most from the ground truth trajectory.

Figure 6: Example image from the planar motion sequence.

7.5 Evaluation on the KITTI Dataset

The KITTI Visual Odometry / SLAM benchmark (Geiger et al., 2012) is a well-known evaluation dataset for SLAM frameworks, and contains several sequences with planar or near planar motion. A large portion of the images depict the roads, on which the car travels, however, one must note that this is only a coarse approximation to the general planar motion model, as all sequences contain non-planar structures to some extent, e.g. passing vehicles, pedestrians, traffic barriers and road signs. This, however, is a good way of testing the robustness of the proposed solvers, as future applications may not entirely fulfill the general planar motion model. Furthermore, in order to be able to consider the input images as depicting a (near) planar scene, a subset of the image is cropped out before estimating the homographies, as is illustrated in Figure 8.

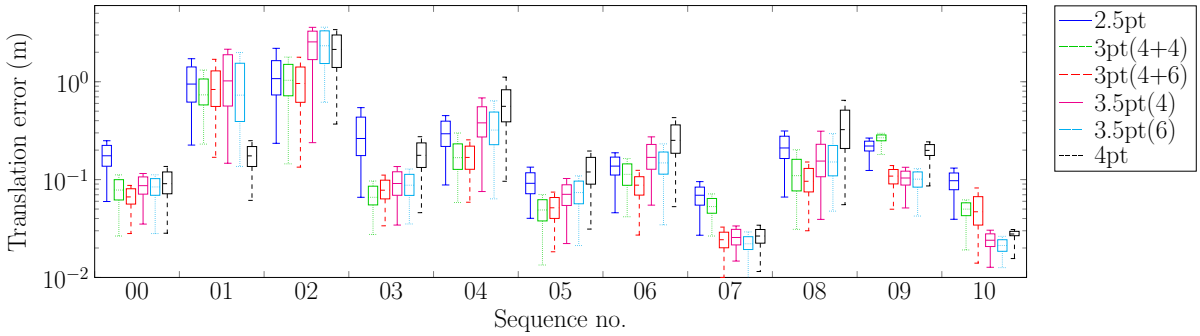

Figure 7: Mean translation error for the first ten images of the first camera of Sequence 00–10 of the KITTI dataset. These are all image sequences containing ground truth. At least on of the proposed solvers have the lowest mean translation error in all but one of the eleven cases. The mean translation error is computed over 500 iterations.

Figure 8: Image from the KITTI Visual Odometry / SLAM benchmark, Sequence 03. The cropped area (contained within the thick border) depict the image used to compute the homographies. Image credit: KITTI dataset (Geiger et al., 2012).

From the cropped images of the first eleven sequences of the KITTI dataset, for which ground truth data is available, the homographies were computed using SURF features, as in the previous experiments. The performance of the solvers was measured as the mean error of the Euclidean distance between the ground truth positions and estimated positions. The results are averaged over 500 tests, and include the first ten images of each sequence. This number was chosen to reduce the impact of error propagation, while still having a noticeable effect of imposing the general planar motion model. The differences of the estimation is due to the matching algorithm as well as the RANSAC framework for estimating the homographies. No non-linear refinement of the homographies were used. The results are shown in Figure 7.

The proposed solvers are robust, and produce a good initial estimate for the trajectory, and at least one of the proposed solvers has the lowest median translation error in all sequences, except Sequence 01.

This result may, to some extent, be unanticipated, however, one must not forget that the conditions for the general planar motion model is not fulfilled in the KITTI dataset. The disadvantage of using the minimal 2.5-point solver, it seems, is that the model is imposed exactly, whereas for the 4-point DLT solver, the model is completely disregarded, and instead are determined solely by the data. One possible answer to the results we observe on the KITTI dataset, which favours the proposed solvers, is that it enforces a weaker form of the general planar motion model (since only one or two of the defining equations are considered) and tunes to the data in cases where the model assumptions are invalid.

8 CONCLUSIONS

In this paper a novel non-minimal polynomial constraint for homographies compatible with the general planar motion model has been derived. A series of non-minimal solvers have been proposed, which enforces one or two of the defining constraints. They have been demonstrated on synthetic and real data to perform well, and two of them are reported to be faster than the minimal solver.

In cases where the general planar motion model is a coarse approximation of the actual scene it is likely that the proposed solvers are more robust, compared to both the minimal solver and the 4-point solver. Hence, it has been demonstrated that pre-maturely enforcing the planar motion model, without incorporating the fixed overhead tilt constraint, does not necessarily yield a better end result.

By incorporating the proposed solver in a complete SLAM system, it is likely that the total execution time will decrease due to a lower number of iterations needed by non-linear refinement of poses and scene points in a bundle adjustment framework.

ACKNOWLEDGMENTS

The author gratefully acknowledges Mårten Wadenbäck and Martin Karlsson for providing the data for the planar motion compatible sequences.

This work has been funded by the Swedish Research Council through grant no. 2015-05639 'Visual SLAM based on Planar Homographies'.

REFERENCES

Chen, T. and Liu, Y.-H. (2006). A robust approach for structure from planar motion by stereo image sequences. *Machine Vision and Applications (MVA)*, 17(3):197–209.

Cox, D. A., Little, J., and O'Shea, D. (2005). *Using Algebraic Geometry*. Graduate Texts in Mathematics. Springer New York.

Fischler, M. and Bolles, R. (1981). Random sample consensus: A paradigm for model fitting with applications to image analysis and automated cartography. *Communications of the ACM*, 24(6):381–395.

Geiger, A., Lenz, P., and Urtasun, R. (2012). Are we ready for autonomous driving? The KITTI vision benchmark suite. *Conference on Computer Vision and Pattern Recognition (CVPR)*, pages 3354–3361.

Grayson, D. R. and Stillman, M. E. (2018). Macaulay2 – a software system for research in algebraic geometry. Available at http://www.math.uiuc.edu/Macaulay2/.

Hajjdiab, H. and Laganière, R. (2004). Vision-based multi-robot simultaneous localization and mapping. In *Canadian Conference on Computer and Robot Vision (CRV)*, pages 155–162, London, ON, Canada.

Hartley, R. I. and Zisserman, A. (2004). *Multiple View Geometry in Computer Vision*. Cambridge University Press, Cambridge, England, UK, second edition.

Kukelova, Z., Bujnak, M., and Pajdla, T. (2008). Automatic generator of minimal problem solvers. *European Conference on Computer Vision (ECCV)*, pages 302–315.

Larsson, V. and Åström, K. (2016). Uncovering symmetries in polynomial systems. *European Conference on Computer Vision (ECCV)*, pages 252–267.

Larsson, V., Åström, K., and Oskarsson, M. (2017a). Efficient solvers for minimal problems by syzygy-based reduction. *Computer Vision and Pattern Recognition (CVPR)*, pages 2383–2392.

Larsson, V., Åström, K., and Oskarsson, M. (2017b). Polynomial solvers for saturated ideals. *International Conference on Computer Vision (ICCV)*, pages 2307–2316.

Larsson, V., Kukelova, Z., and Zheng, Y. (2018a). Camera pose estimation with unknown principal point. *Computer Vision and Pattern Recognition (CVPR)*, pages 2984–2992.

Larsson, V., Oskarsson, M., Åström, K., Wallis, A., Kukelova, Z., and Pajdla, T. (2018b). Beyond gröbner bases: Basis selection for minimal solvers. *Computer Vision and Pattern Recognition (CVPR)*, pages 3945–3954.

Liang, B. and Pears, N. (2002). Visual navigation using planar homographies. In *International Conference on Robotics and Automation (ICRA)*, pages 205–210, Washington, DC, USA.

Möller, H. M. and Stetter, H. J. (1995). Multivariate polynomial equations with multiple zeros solved by matrix eigenproblems. *Numerische Mathematik*, 70(3):311–329.

Ortín, D. and Montiel, J. M. M. (2001). Indoor robot motion based on monocular images. *Robotica*, 19(3):331–342.

Torr, P. H. S., Zisserman, A., and Maybank, S. J. (1998). Robust detection of degenerate configurations while estimating the fundamental matrix. *Computer Vision and Image Understanding*, 71(3):312 – 333.

Trefethen, L. and Bau, D. (1997). *Numerical Linear Algebra*. SIAM.

Triggs, B. (1991). Camera pose and calibration from 4 or 5 known 3d point. *International Conference on Computer Vision (ICCV)*, pages 278–284.

Ventura, J., Arth, C., Reitmayr, G., and Schmalstie, D. (2014). A minimal solution to the generalized pose-and-scale problem. *Computer Vision and Pattern Recognition (CVPR)*, pages 422–429.

Wadenbäck, M. and Heyden, A. (2013). Planar motion and hand-eye calibration using inter-image homographies from a planar scene. *International Conference on Computer Vision Theory and Applications (VISAPP)*, pages 164–168.

Wadenbäck, M. and Heyden, A. (2014). Ego-motion recovery and robust tilt estimation for planar motion using several homographies. *International Conference on Computer Vision Theory and Applications (VISAPP)*, pages 635–639.

Wadenbäck, M., Åström, K., and Heyden, A. (2016). Recovering planar motion from homographies obtained using a 2.5-point solver for a polynomial system. *International Conference on Image Processing (ICIP)*, pages 2966–2970.

Zheng, Y., Kuang, Y., Sugimoto, S., Åström, K., and Okutomi, M. (2013). Revisiting the pnp problem: A fast, general and optimal solution. *International Conference on Computer Vision (ICCV)*, pages 2344–2351.

Zienkiewicz, J. and Davison, A. J. (2015). Extrinsics autocalibration for dense planar visual odometry. *Journal of Field Robotics (JFR)*, 32(5):803–825.

APPENDIX

Synthetic Experiments

Re-projection Error

In (Wadenbäck et al., 2016) the re-projection error for the point correspondences not used in order to obtain the estimated homographies were analysed, and we reproduce it here together with the proposed solvers. As seen in Figure 9, the trend is similar to what was observed in the previous case (cf. Frobenius norm estimate, Figure 3) namely, the median re-projection er-

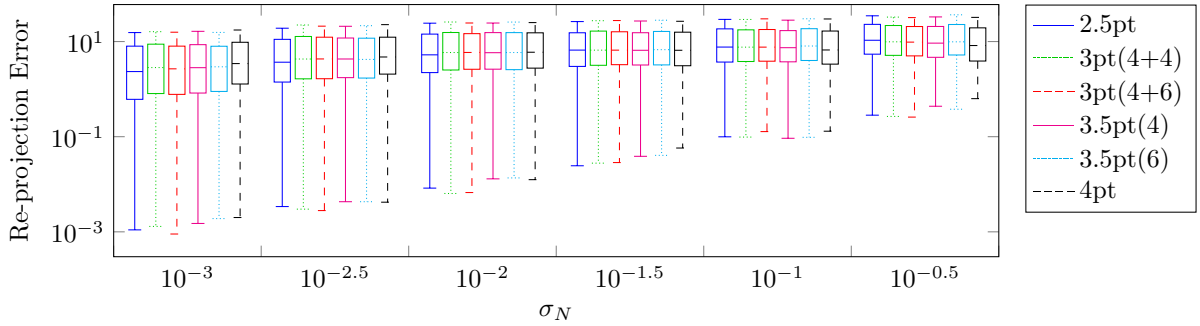

Figure 9: Mean re-projection error for different noise levels σ_N. Similar to Figure 3 the median value for the proposed solvers is between the corresponding values for the 2.5-point solver and DLT; however, for higher noise levels, we note an advantage for the non-minimal solvers and DLT compared to the minimal 2.5-point solver.

rors for the non-minimal solvers are between the corresponding values of the minimal 2.5-point solver and the 4-point solver (DLT) for all noise levels. Note, however, that for large noise levels, the 2.5-point solver does not perform as well as the non-minimal solvers or the traditional 4-point solver.

Motion Parameters

Additional plots for the second synthetic experiment, regarding the estimation of the motion parameters, is shown in Figure 11. The mean errors are for noise level $\sigma_N = 10^{-2}$. In Figure 12 the same parameters, but for $\sigma_N = 10^{-1}$ are shown.

Synthetic Images

Example images that were used in the synthetic image experiment is shown in Figure 10, and example output for the reconstructed path is shown in Figure 13 for all solvers. Neither the 4pt solver, nor the minimal solver performs best in this case.

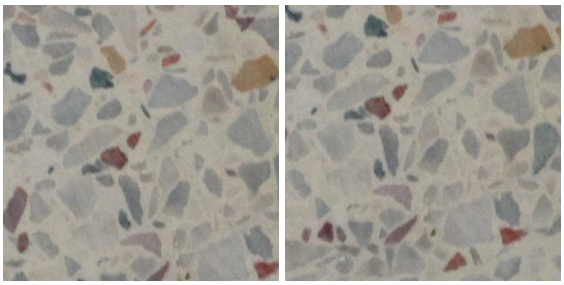

Figure 10: Two consecutive images from the synthetic dataset.

Experiments on Real Data

Planar Motion

We here show two more test cases conducted with the omnidirectional robot rob@work, from Section 7.4. In the first test case the robot moves forward (in relation to its own frame), while rotating, thus creating a light turn. The sequence contains 344 images. In the second test case the robot simulates a sequences of parallel parking, by first driving straight and then making a sharp turn, while keeping the orientation constant. This sequence contains 325 images. The estimated paths are shown in Figure 14.

KITTI Dataset

To demonstrate some qualitative usage of the proposed solvers, four longer subsequences of the KITTI dataset were evaluated, see Figure 15. Only the $3pt(4+4)$ solver is shown in order to make the plots legible. For sequences of this length it is customary to use bundle adjustment, or some other non-linear refinement that minimize a physically meaningful error such as the geometric re-projection error or photometric error. In order for such optimization schemes to converge in a reasonable amount of time it is often necessary to supply a good initial guess of the trajectory. Due to the reduced computational complexity, comparable to using the 4-point DLT solver, when considered in a RANSAC framework, and the qualitative performance on the KITTI dataset, we find the proposed 3-point solver to be a suitable alternative to be incorporated in a SLAM system.

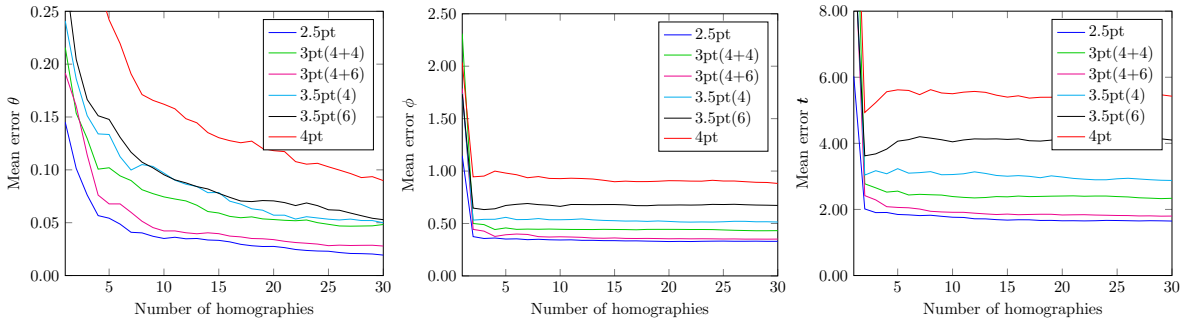

Figure 11: Mean error for θ, ϕ (in degrees) and $\boldsymbol{t}$ for 100 iterations with $\sigma_N = 10^{-2}$.

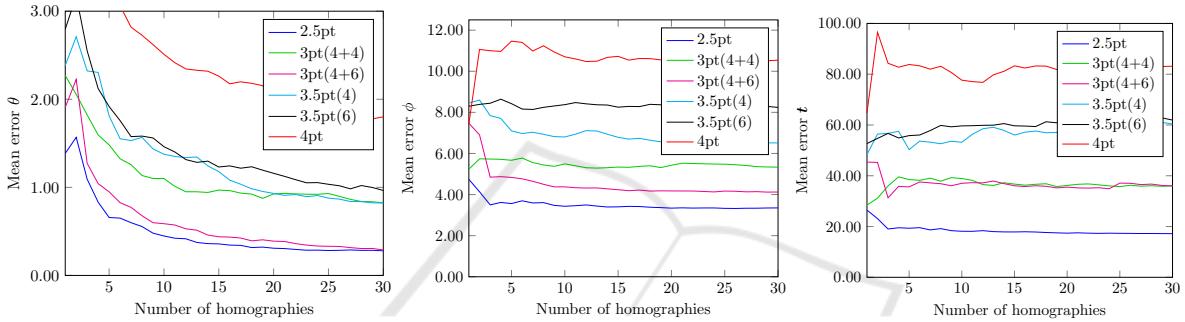

Figure 12: Mean error for θ, ϕ (in degrees) and $\boldsymbol{t}$ for 100 iterations with $\sigma_N = 10^{-1}$.

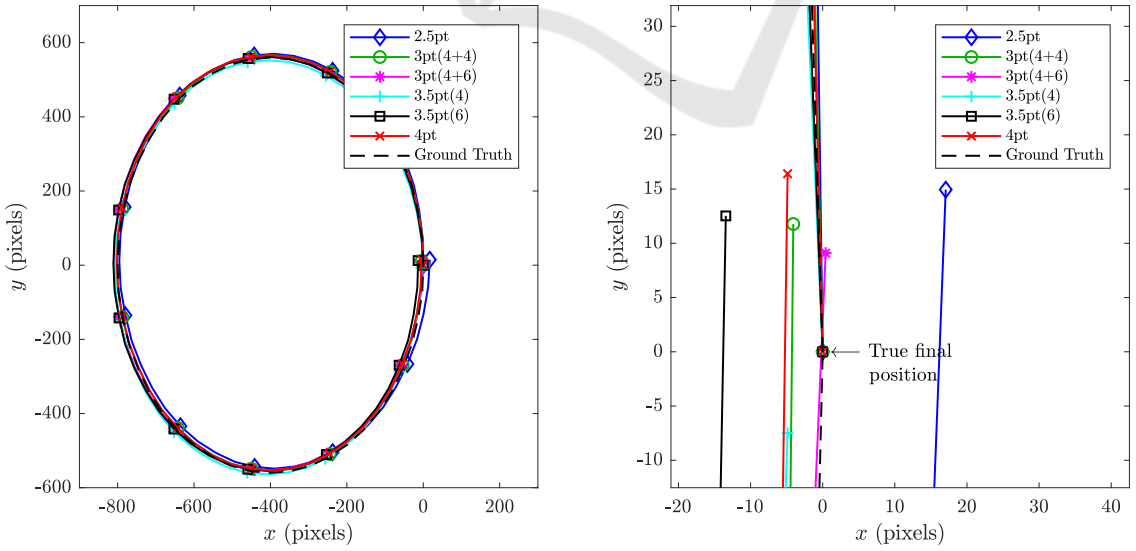

Figure 13: Example of reconstructed path for the synthetic image sequence for all solvers, and zoomed in at the final position (right image).

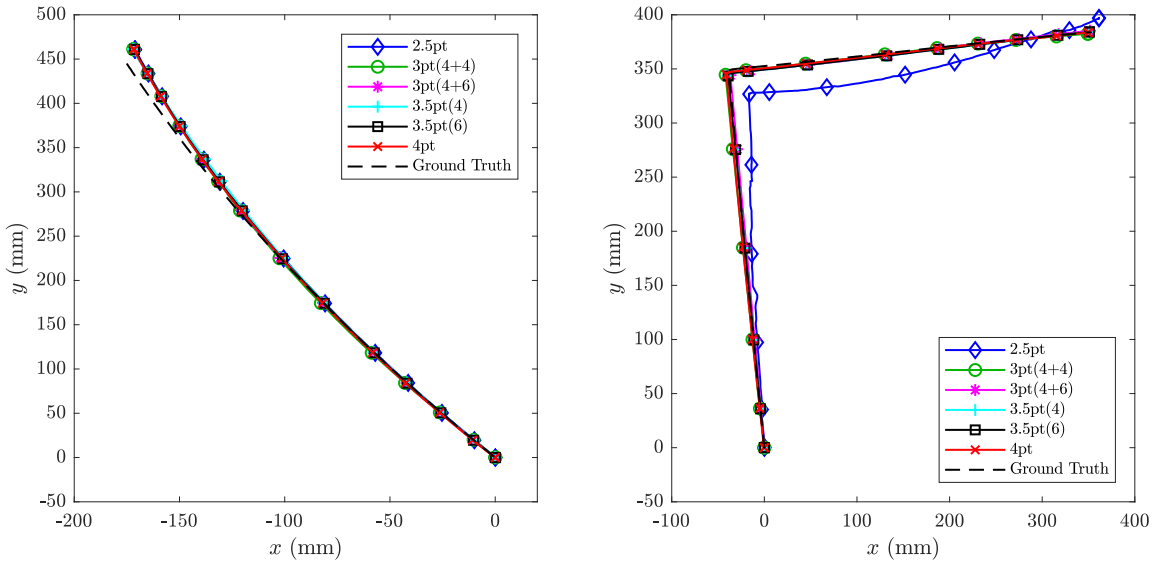

(a) . (b) .

Figure 14: Estimated trajectories of the mobile robot used in the planar motion experiments for the "turn" experiment (left) and the "parallel parking" experiment.

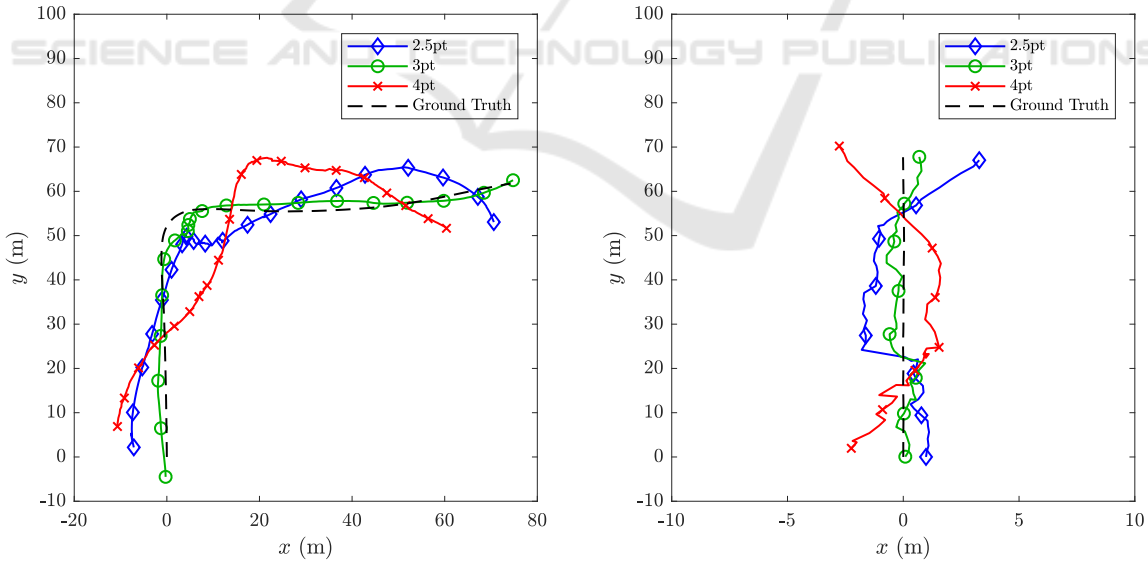

(a) Sequence 03 (200 images). (b) Sequence 04 (50 images).

Figure 15: Estimated trajectories of subsequences of Sequence 03 and 04 of the KITTI dataset. Procrustes analysis has been carried out to align the estimated trajectories with the ground truth. Note that the aspect ratio differs between sequences, in order to clearly visualize the differences between the estimated trajectories. No non-linear refinement has been carried out in any of the test cases. The 3-point solver used is the 3pt(4+4) solver.